Title
Exploiting Lithium–Ether Co-Intercalation in Graphite for High-Power Lithium-Ion Batteries

Permalink

Journal
Advanced Energy Materials, 7(19)

ISSN
1614-6832

Authors
Kim, Haegyeom
Lim, Kyungmi
Yoon, Gabin
et al.

Publication Date
2017-10-01

DOI
10.1002/aenm.201700418

Peer reviewed

FULL PAPER

Lithium-Ion Batteries

ADVANCED
ENERGY
MATERIALS

www.advenergymat.de

Exploiting Lithium–Ether Co-Intercalation in Graphite for High-Power Lithium-Ion Batteries

*Haegyeom Kim, Kyungmi Lim, Gabin Yoon, Jae-Hyuk Park, Kyojin Ku, Hee-Dae Lim, Yung-Eun Sung, and Kisuk Kang**

The intercalation of lithium ions into graphite electrode is the key underlying mechanism of modern lithium-ion batteries. However, co-intercalation of lithium-ions and solvent into graphite is considered undesirable because it can trigger the exfoliation of graphene layers and destroy the graphite crystal, resulting in poor cycle life. Here, it is demonstrated that the [lithium–solvent]+ intercalation does not necessarily cause exfoliation of the graphite electrode and can be remarkably reversible with appropriate solvent selection. First-principles calculations suggest that the chemical compatibility of the graphite host and [lithium–solvent]+ complex ion strongly affects the reversibility of the co-intercalation, and comparative experiments confirm this phenomenon. Moreover, it is revealed that [lithium–ether]+ co-intercalation of natural graphite electrode enables much higher power capability than normal lithium intercalation, without the risk of lithium metal plating, with retention of ≈87% of the theoretical capacity at current density of 1 A g−1. This unusual high rate capability of the co-intercalation is attributed to the (i) absence of the desolvation step, (ii) negligible formation of the solid–electrolyte interphase on graphite surface, and (iii) fast charge-transfer kinetics. This work constitutes the first step toward the utilization of fast and reversible [lithium–solvent]+ complex ion intercalation chemistry in graphite for rechargeable battery technology.

1. Introduction

Graphite can serve as an intercalation host for versatile guest species in its galleries, forming binary/ternary graphite intercalation compounds.[1] Its capability of accommodating lithium ions via intercalation combined with its low cost and abundance has made graphite a standard anode for modern lithium-ion batteries (LIBs).[2–6] In the early development of LIBs employing graphite anodes, the search for an appropriate electrolyte system was important with respect to not only the ionic conductivity and/or electrochemical window but also its compatibility with the graphite anode.[7–13] The use of propylene carbonate (PC)-based electrolytes resulted in rapid capacity degradation of graphite anodes during battery operation despite their high electrochemical stability.[14,15] Researchers observed that the degradation was related to the co-intercalation of lithium ions and the large solvent molecules, which led to exfoliation of the graphene layers.[14,16–18] Thus, subsequent efforts have been made to prevent co-intercalation in graphite anodes for LIBs, which naturally led to the perception that ion–solvent co-intercalation is detrimental in this system.[16,17,19] However, recently, Kim et al.[20] and Jache and Adelhelm[21] independently reported the potential of graphite as an anode material for sodium-ion batteries (NIBs) by employing the co-intercalation of sodium ions and solvent molecules. In this system, graphite accommodated the intercalation of [sodium–ether]+ complex ions without noticeable side reactions such as the exfoliation of graphite. Moreover, the graphite anode provided superior cycle stability (more than 2500 repetitive electrochemical cycles), demonstrating the reversibility of the co-intercalation chemistry despite the large volume expansion of ≈345%.[20–23] Subsequent research conducted by Cui and co-workers also demonstrated the practical feasibility of [sodium–ether]+ complex ion intercalation in NIBs and sodium-ion capacitors with good cycle stability.[24,25]

Our current study started from a simple question of the contradiction between reversible [sodium–solvent]+ co-intercalation and well-known instability of [lithium–solvent]+ co-intercalation in graphite electrodes.[16,20–22,26] Although lithium and sodium

Dr. H. Kim,[+] K. Lim, G. Yoon, K. Ku, Dr. H.-D. Lim,[++] Prof. K. Kang
Department of Materials Science and Engineering
Research Institute of Advanced Materials (RIAM)
Seoul National University
1 Gwanak-ro, Gwanak-gu, Seoul 151-742, Republic of Korea
E-mail: matlgen1@snu.ac.kr

The ORCID identification number(s) for the author(s) of this article can be found under https://doi.org/10.1002/aenm.201700418.

[+]Present address: Materials Science Division, Lawrence Berkeley National Laboratory, Berkeley, CA 94720, USA

[++]Present address: Department of NanoEngineering, University of California, San Diego, La Jolla, CA 92093, USA

G. Yoon, J.-H. Park, Prof. Y.-E. Sung, Prof. K. Kang
Center for Nanoparticle Research
Institute for Basic Science (IBS)
Seoul National University
1 Gwanak-ro, Gwanak-gu, Seoul 151-742, Republic of Korea

J.-H. Park, Prof. Y.-E. Sung
School of Chemical and Biological Engineering
Seoul National University
1 Gwanak-ro, Gwanak-gu, Seoul 151-742, Republic of Korea

**ADVANCED
SCIENCE NEWS**
www.advancedsciencenews.com

**ADVANCED
ENERGY
MATERIALS**
www.advenergymat.de

share similar chemical and electrochemical properties to some extent, they exhibit surprisingly distinct behaviors in the co-intercalation. Moreover, the origin of the severe exfoliation of graphite associated with the lithium ion–solvent complex despite the smaller size of lithium ions compared with sodium ions is unclear. This work unveils the importance of the chemical compatibility of the co-intercalated solvent in determining whether exfoliation occurs in the lithium co-intercalation. In addition, it is demonstrated that the [lithium–ether]$^+$ complex ion de/intercalation in graphite is remarkably reversible, enabling a cycle life of more than 200 cycles, and that the previously reported instability of ether-based lithium co-intercalation is not due to the intrinsic irreversibility in graphite.[26] Furthermore, the graphite electrode based on the co-intercalation is shown to be capable of delivering a high power capability, retaining ≈87% of its theoretical capacity at a current density of 1 A g^{-1} without the risk of lithium metal plating. The observed high power capability of the co-intercalation is counterintuitive, considering that the intercalation of large guest ions in the host has been believed to be sluggish. The origin of this unusual phenomenon is discussed in relation to the desolvation kinetics, nature of the solid electrolyte interphase (SEI) layer, and charge storage mechanism.

2. Results and Discussion

The electrochemical behavior of lithium co-intercalation in graphite was examined using an ether-based electrolyte as shown in **Figure 1**a, which presents the discharge/charge profile using 1 M lithium trifluoromethanesulfonate (LiTF) in diethylene glycol dimethyl ether (DEGDME).[23,26] The overall profile in the first cycle clearly differs from the characteristic lithium ion intercalation in conventional LIBs but agrees with the previous report of lithium ion/solvent molecule co-intercalation and is similar to that of the typical [sodium–ether]$^+$ complex ion intercalation shown in Figure 1b.[20,26] However, the specific capacity decreases rapidly during repeated battery cycling; only a fraction of the initial capacity (≈20 mA h g^{-1}) was maintained after 20 cycles, which is consistent with previous
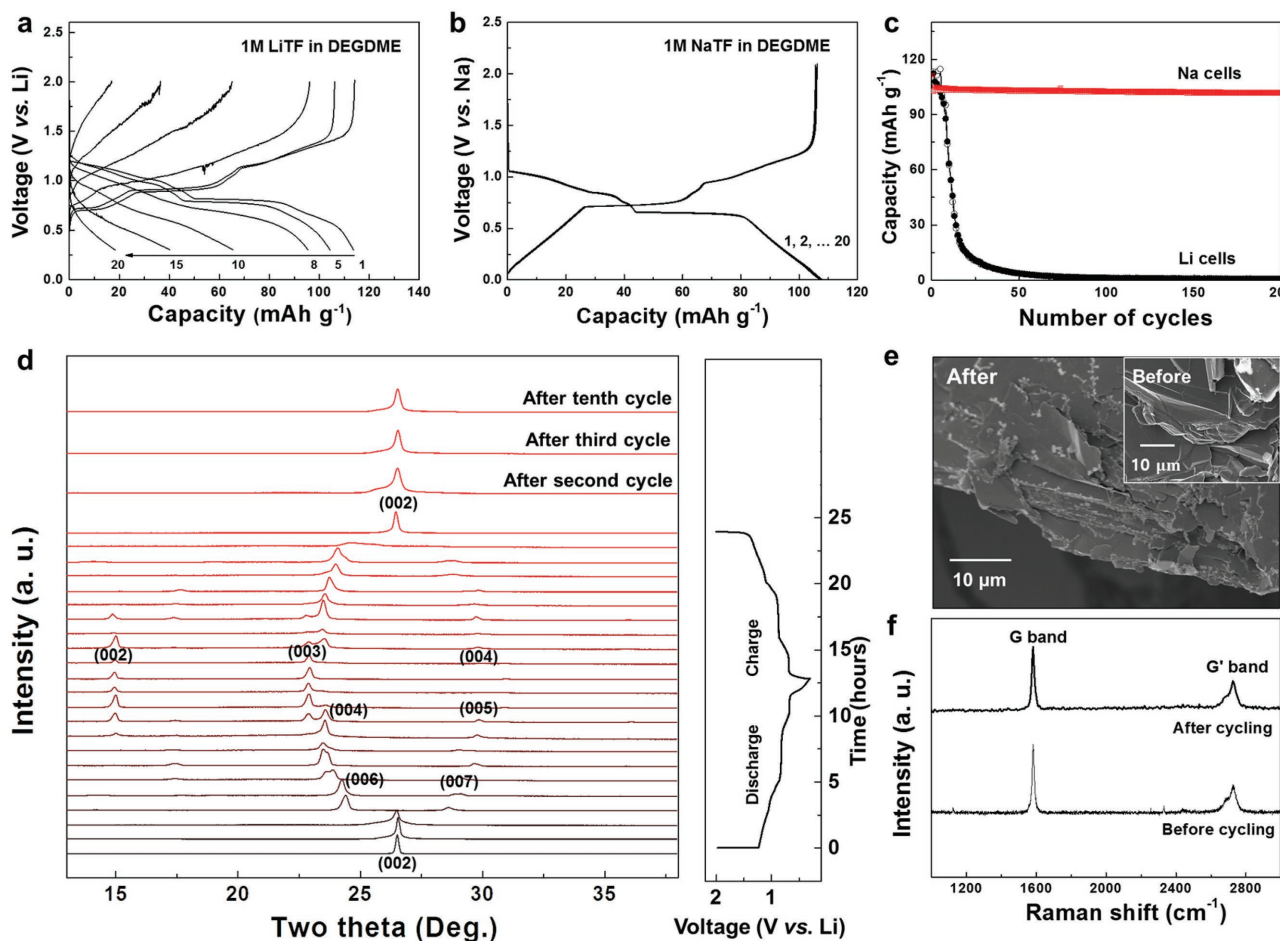

Figure 1. a) Charge/discharge profiles of graphite/lithium cells using 1 M LiTF in DEGDME electrolyte. b) Typical charge/discharge profiles of [sodium–ether]$^+$ complex co-intercalation using 1 M NaTF in DEGDME. c) Cycle performance of graphite anode in sodium and lithium cells using DEGDME electrolytes (black: 1 M LiTF in DEGDME; red: 1 M NaTF in DEGDME). d) Ex situ XRD analysis of the structural evolution of [lithium–ether]$^+$ complex co-intercalation during intercalation and deintercalation into/out of graphite. XRD patterns of graphite after second, third, and tenth cycles are also shown. e) SEM image of graphite electrode after cycling with 1 M LiTFSI in DEGDME (inset: pristine graphite before cycling). f) Raman spectroscopy of the graphite electrode before (bottom) and after (top) cycling.

**ADVANCED
SCIENCE NEWS**
www.advancedsciencenews.com

**ADVANCED
ENERGY
MATERIALS**
www.advenergymat.de

speculations.[16,26] Changing the salt in the electrolyte from LiTF to lithium trifluoromethanesulfonimide (LiTFSI) for improved chemical stability[27,28] did not improve the cycle stability, as observed in Figure S1 (Supporting Information). In contrast, changing the salt from LiTF to NaTF, i.e., [sodium–ether]+ complex ion intercalation, dramatically improved the cycle performance by more than 200 times using the same cell configuration (Figure 1c).[20–22]

To understand this distinct behavior of the graphite electrode, we first characterized the structural change upon repeated lithium co-intercalation in the ether-based electrolyte using ex situ X-ray diffraction (XRD), as shown in Figure 1d. The XRD patterns for the first cycle indicate that the graphite electrode undergoes successive phase transformations, which is consistent with our previous work.[26] The evolution of the XRD patterns is analogous to that of [sodium–ether]+ complex ion intercalation into graphite, indicating a typical co-intercalation staging phenomenon.[26,29] The expansion along the c-axis is slightly smaller for lithium than for sodium during the co-intercalation (≈334% and 349%, respectively, in Figure S2a,b of the Supporting Information).[26] Interestingly, Figure 1d shows that the graphite crystal structure did not undergo any noticeable degradation with the repeated cycles. The XRD patterns of the graphite electrode were nearly unchanged, and the pristine layered structure was maintained after 2, 3, and 10 cycles of the co-intercalation. This finding contradicts the observation that significant cycle degradation occurs after 10 cycles, as shown in Figure 1a,c, suggesting that the structural degradation of the graphite crystal may not be the main cause of the instability of the lithium cells. We further confirmed that no noticeable morphological change (i.e., exfoliation) occurred in the cycled graphite electrode in the ether-based lithium cell, as shown in Figure 1e, which indicates that the morphology of the pristine graphite was well preserved after cycling. No significant increase of the structural defects in the graphite was detected by Raman spectroscopy analysis after the repeated lithium ion co-intercalation (Figure 1f).

The structural integrity of the graphite observed in Figure 1d–f was unexpected, considering the previous observation in PC-based lithium cells, where the graphite became severely exfoliated during the lithium–PC co-intercalation.[14,30] To better understand these contradictory results, we performed first-principles calculations to probe the relative stability of the [lithium–solvent]+ complex ions in the graphite host using different solvents. **Figure 2**a compares the highest occupied molecular orbital/lowest unoccupied molecular orbital (HOMO/LUMO) levels and binding energies of [Li–DEGDME]+ and [Li–PC]+ complex ions. The [Li–DEGDME]+ complex ion exhibits a higher LUMO level than that of [Li–PC]+, and importantly, the Fermi energy of graphite lies well below the LUMO level of [Li–DEGDME]+ but above that of [Li–PC]+. According to previous first-principles calculations, comparison of the LUMO level of a [Na–solvent$_x$]+ complex and the Fermi energy of the host can hint at the relative stability of the co-intercalation.[31,32] When the Fermi energy of the host is higher than the LUMO level of the complex, downhill electron energy transfer may occur from the graphite host to the solvent molecule, which can subsequently trigger a parasitic chemical reaction between the two components.[31,32] This finding implies that the [Li–PC]+

complex would be unstable and possibly undergo chemical reactions with the graphite host, whereas the [Li–DEGDME]+ complex would be stable in the graphite galleries (Figure 2b). Furthermore, DEGDME shows stronger binding with lithium ions than PC in Figure 2a, inferring more robust solvation of lithium ions in the graphite host.

Our experimental results were consistent with the prediction from the calculations. We observed that [Li–PC]+ is not stable in the graphite galleries and that a substantial amount of carbon-containing gas evolved during the co-intercalation, whereas the intercalation of [Li–DEGDME]+ did not induce this gas evolution. Figure 2c,d, and Figure S3 (Supporting Information) present in situ mass spectrometry analyses of the graphite electrodes with the PC and DEGDME electrolyte systems, respectively (see Figure S4 of the Supporting Information for the experimental setup). During the discharge in the Li–PC electrolyte system in Figure 2c, gas-phase byproducts such as propene, CO_2, CO, and H_2 (shaded with yellow) were clearly detected. However, no noticeable gas evolution was observed in the Li–DEGDME electrolyte system during the discharge and subsequent charge (Figure 2d), which is consistent with the observed structural integrity of the graphite electrode in the DEGDME electrolyte in Figure 1e,f. The scanning electron microscopy (SEM) results presented in Figure 2e reveal that gas evolution accompanied severe exfoliation of graphite during [Li–PC]+ complex ion intercalation in graphite galleries (see Figure S5 for additional SEM images of the exfoliated graphite using the PC-based electrolyte) unlike for the Li–DEGDME electrolyte system. Moreover, the intensity of the characteristic graphite (002) peak of the XRD pattern was significantly reduced after the cycle, as observed in Figure 2f. These results strongly suggest that the gas evolution within the graphite interlayer with the PC electrolyte could trigger the exfoliation of graphite and degradation of the crystal structure, as schematically proposed in Figure 2b.

We discovered that the observed capacity degradation for ether-based lithium cells did not originate from the degradation of the graphite electrode due to the [lithium–ether]+ co-intercalation itself but simply stemmed from the degradation of the lithium metal counter electrode during the electrochemical cycling. **Figure 3**a reveals that the lithium metal counter electrodes were covered with dark brown films after repeated battery cycling using both LiTF and LiTFSI in DEGDME, indicating severe side reactions.[33,34] The SEM images in Figure 3b also confirm that the surface of lithium metal was passivated by unknown byproducts after the cycling with the ether-based electrolyte. According to the energy dispersive spectroscopy (EDS) analyses in Figure 3c,d, the byproducts mainly consisted of carbon, oxygen, sulfur, and fluorine, which are the major constituting elements of the electrolyte, indicating electrolyte decomposition. Further characterization of the film using X-ray photoemission spectroscopy (XPS), as shown in Figure 3e, revealed the presence of mixed products with CF_3–O, CF_2–CH_2, O–C=O, C–O, and C–C bonding, supporting the speculation of a chemical reaction between the DEGDME and lithium metal.[34] However, no noticeable change was detected on the sodium metal surface after the cell was cycled with the ether-based electrolyte (Figure S6, Supporting Information). This clear difference in the metal surface suggests that the instability
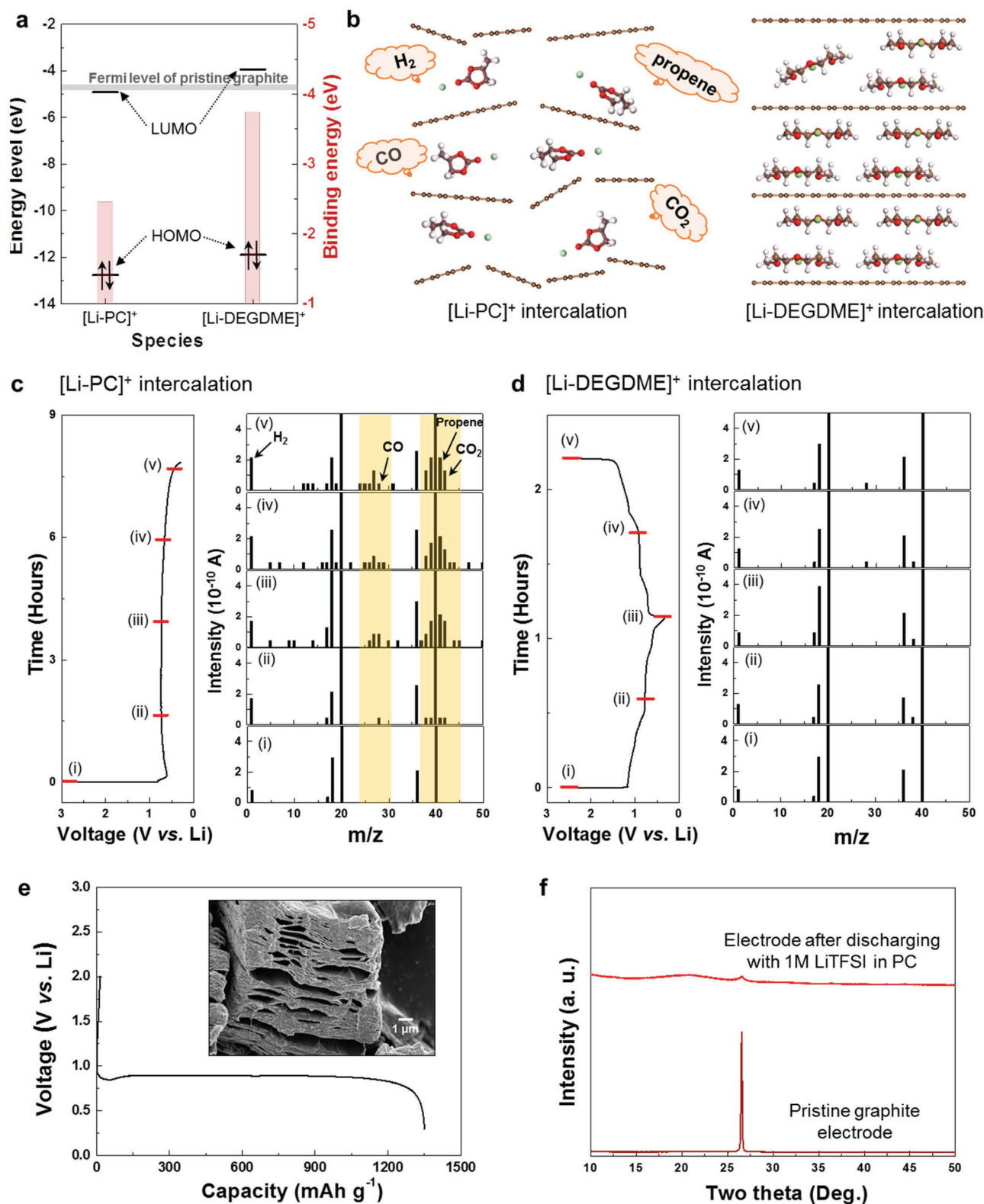
Figure 2. a) Comparison of LUMO and HOMO levels with the Fermi level of graphite and binding energy of lithium–solvents (left *y*-axis: energy level, right *y*-axis: binding energy). b) Schematic illustrations of lithiated graphite electrode using PC and DEGDME electrolytes. Gas evolution analyses during battery operations in c) PC and d) DEGDME electrolyte systems. The mass-to-charge ratio (*m/z*) on the *x*-axis represents the mass of the evolved gas molecules. e) Typical charge/discharge profile of graphite electrode using 1 M LiPF$_6$ in PC electrolyte (inset: SEM image of graphite after cycling). f) XRD patterns of pristine graphite electrode and electrode after discharge with 1 M LiTFSI in PC.
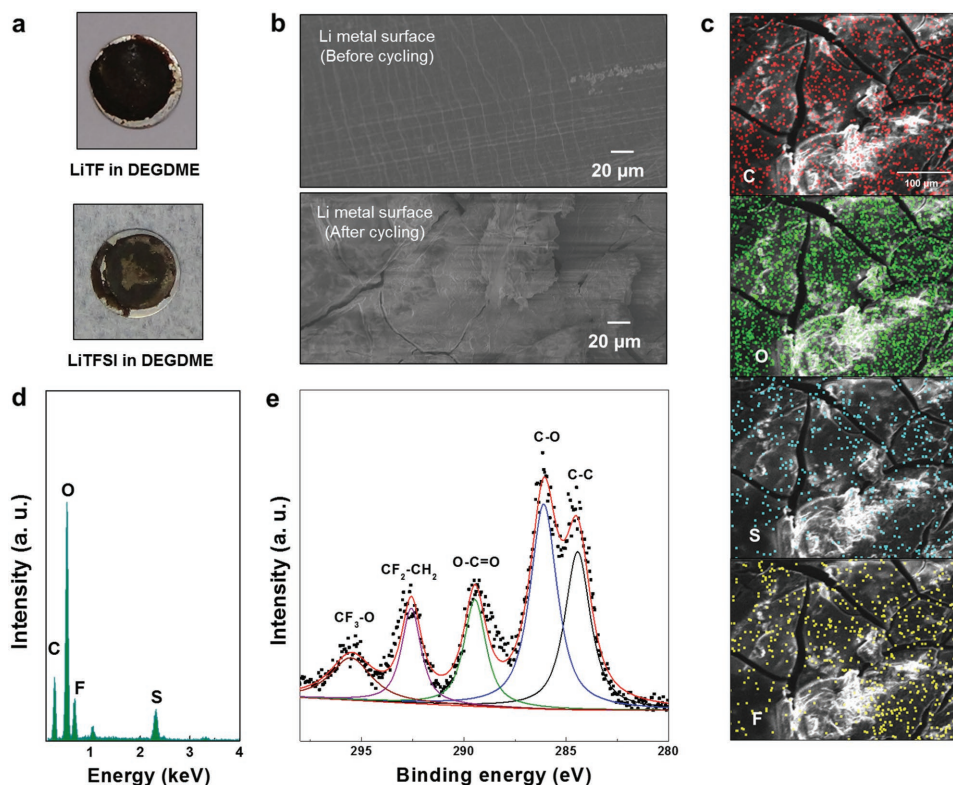
ADVANCED
SCIENCE NEWS
www.advancedsciencenews.com

ADVANCED
ENERGY
MATERIALS
www.advenergymat.de

Figure 3. Photoimages of lithium metal and separators after battery operation in a) 1 M LiTF in DEGDME (top) and 1 M LITFSI in DEGDME (bottom) electrolytes. b) SEM images of lithium metal before and after battery operation. c) EDS mapping, d) EDS spectrum, and e) XPS analyses of lithium metal after battery operation with 1 M LiTFSI in DEGDME.

of the lithium metal electrode in the electrolyte caused the capacity degradation, particularly for the lithium cells. In a separate experiment, we further confirmed the chemical incompatibility of the lithium metal with the DEGDME-based electrolyte, as shown in Figure S7 (Supporting Information). The DEGDME-based electrolyte turned dark brown after being used to store lithium metal for 72 h, indicating that lithium metal is chemically unstable with DEGDME-based electrolytes, i.e., 1 M LiTF and 1 M LiTFSI in DEGDME. In contrast, no significant changes were observed for carbonate-based electrolytes, i.e., 1 M lithium hexaflourophosphate ($LiPF_6$) in ethylene carbonate/dimethylene carbonate (EC/DMC) and 1 M LiTFSI in EC/DMC, in the same experiment (Figure S7, Supporting Information). Based on these results, a graphite/lithium metal cell was assembled with 1 M LiTFSI in DEGDME and rested it for 72 h, followed by charging/discharging (Figure S8, Supporting Information). It revealed that the capacity decreases much more rapidly in the 72 h rested cell than the immediately cycled cell (Figure S1, Supporting Information), confirming again that capacity degradation is attributable to the severe side reaction between lithium metal and the electrolyte. The incompatibility of lithium metal with the DEGDME electrolyte in the electrochemical cell was additionally confirmed for lithium metal cells employing a $Li_4Ti_5O_{12}$ (LTO) electrode (vs lithium metal electrode), which underwent rapid capacity degradation, as observed in Figure S9 (Supporting Information). Inspired by this finding, we attempted to minimize the chemical reaction between the DEGDME-based electrolyte and lithium metal and

reinvestigated the cycling performance of the graphite electrode based on the co-intercalation. Figure S10 (Supporting Information) compares the cycle properties of graphite electrode cells with and without lithium nitrate ($LiNO_3$) additives in the electrolyte. The addition of $LiNO_3$ results in a chemical protection layer on the lithium metal surface against the electrolyte after the initial battery cycling.[35,36] The cycle performance was significantly enhanced with the $LiNO_3$ additive, providing further evidence of the chemical reaction between the DEGDME-based electrolyte and lithium metal in the previously observed rapid capacity degradation of electrochemical cells containing the co-intercalating graphite electrode.

The electrochemical property of the graphite electrode based on the co-intercalation is further explored in **Figure 4**. First, to verify the practical feasibility of the graphite co-intercalation, a full cell was assembled with a $LiFePO_4$ (LFP) cathode and graphite anode in a DEGDME-based electrolyte. Figure 4a presents typical charge/discharge profiles of the cell, which demonstrate that the characteristic profiles of both $LiFePO_4$ and graphite were observed in the full cell and were not altered upon repeated battery cycling. In addition, no color change indicating side reaction was observed in the separator of the graphite/LFP cell whereas the separator of graphite/lithium metal cell turned black (Figure S11, Supporting Information). The full cell retained ≈80% of the initial discharge capacity even after 200 cycles (Figure 4b), validating that the [Li–DEGDME]$^+$ complex ion intercalation in the graphite is highly reversible and applicable as a full cell. To further understand

**ADVANCED
SCIENCE NEWS**

www.advancedsciencenews.com

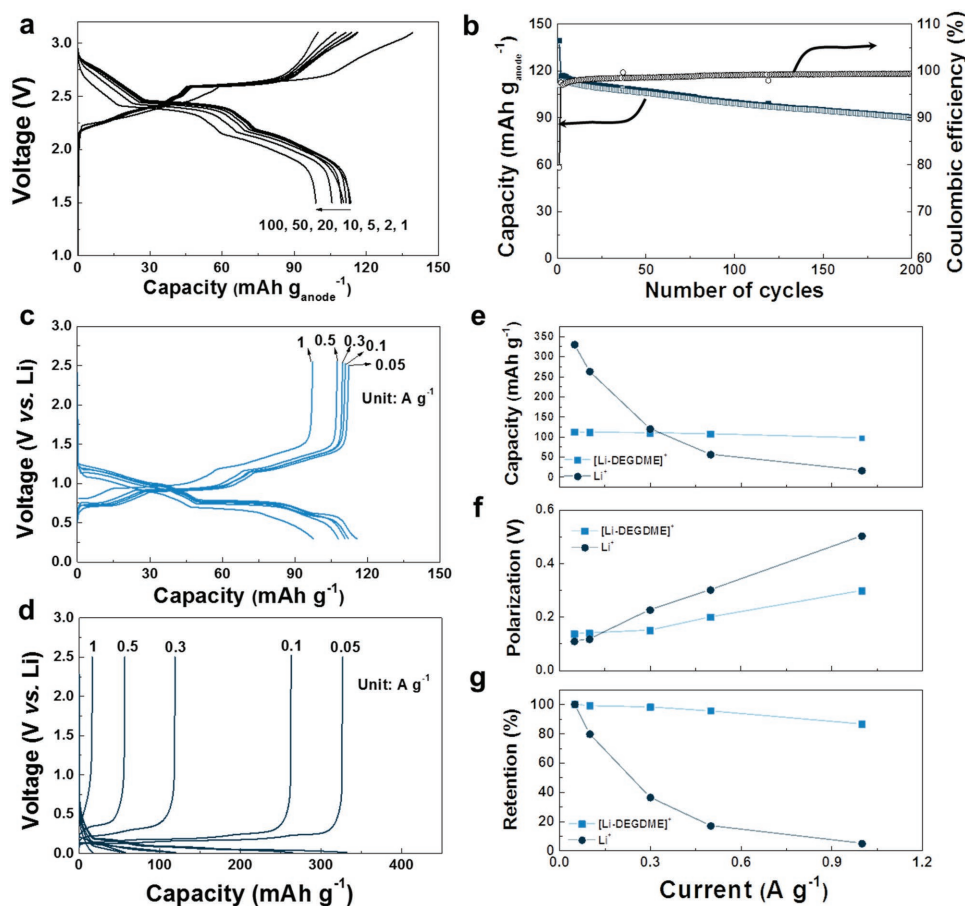**ADVANCED
ENERGY
MATERIALS**

www.advenergymat.de

Figure 4. a) Charge/discharge profiles and b) cycle stability of LiFePO$_4$/graphite cells. Rate capability of the graphite electrode in c) 1 M LiTFSI in DEGDME and d) 1 M LiPF$_6$ in EC/DMC (1:1, v/v) electrolytes. Comparison of rate capability in terms of e) capacity, f) polarization, and g) capacity retention.

the co-intercalation, the electrochemical performance of the graphite electrode was compared with that of conventional lithium-ion intercalation, as shown in Figure 4c,d. Despite the fact that the theoretical capacity of [Li–DEGDME]$^+$ complex co-intercalation is lower than that of conventional lithium-ion intercalation probably due to the space occupancy of the lithium solvating molecules in graphite galleries, the co-intercalation-based reaction was capable of delivering a much higher power capability than the conventional lithium ion intercalation using graphite with an ≈100 μm particle size. The [Li–DEGDME]$^+$ co-intercalation into the graphite could be performed up to 1 A g^{-1} (charge time <6 min) without a significant reduction of the capacity, which is consistent with our previous findings.[26] In contrast, a negligible capacity was achieved for the conventional lithium ion intercalation at 1 A g^{-1}. Figure 4e plots the specific capacities of the two cells as a function of the current rates. Although the normal lithium ion intercalation into graphite delivered higher capacity than the co-intercalation at low current densities, the capacity decreased dramatically with increasing current rate. However, the deliverable capacity from the co-intercalation remained nearly constant irrespective of the current rates and even exceeded that of the conventional lithium ion intercalation for currents greater than 0.5 A g^{-1}. The faster kinetics of the co-intercalation into graphite is also supported by

the smaller increase in the polarization between the charge and discharge with increasing current in Figure 4f. At low current rates, the polarizations were almost identical for both cases; however, the polarization of the co-intercalation became much lower at high current rates. At the 1 A g^{-1} rate, the polarization between the charge and discharge was as low as 0.3 V for the co-intercalation, which is only half of the value for the normal lithium ion intercalation. In Figure 4g, the rate capability is compared in terms of the normalized capacity retention, demonstrating that the co-intercalation is capable of retaining ≈87% of the theoretical capacity at 1 A g^{-1}. For a more practical feasibility comparison, we assessed the energy densities for the co-intercalation and normal intercalation in the full cell setup with LiFePO$_4$ as a cathode (Figure S12, Supporting Information). The gravimetric/volumetric energy density of the co-intercalation eventually exceeded that of the conventional intercalation at current rates above 0.5 A g^{-1}, highlighting the viability of the co-intercalation-based graphite electrode for high-power energy storage devices, even with a slightly higher electrolyte price of ether-based electrolyte (Table S1, Supporting Information). However, it should be noted that the electrolyte accounts for ≈8% of the total battery price,[37] thus it is believed that the cost difference would not be substantial. Additionally, the energy density of [Li–DEGDME]$^+$ co-intercalation was compared with

ADVANCED
SCIENCE NEWS
www.advancedsciencenews.com

ADVANCED
ENERGY
MATERIALS
www.advenergymat.de

$Li_4Ti_5O_{12}$, a widely known electrode material for its high power capability. [Li–DEGDME]$^+$ co-intercalation exhibits similar gravimetric energy density compared to $Li_4Ti_5O_{12}$, but it was found that the co-intercalation graphite is capable of providing more merits in delivering higher practical volumetric energy density than $Li_4Ti_5O_{12}$ considering all cell components including conductive agents, binder and current collector (Figure S12d,e, Supporting Information). While there were not particular difference regarding the binder and the current collector, a larger amount of conducting agent was inevitable to prepare the LTO electrode owing to its intrinsic low electronic conductivity compared to the graphite. Both full cells showed stable cycle life as demonstrated in Figure S13 (Supporting Information). Note that the high power capability of the graphite electrode can be beneficial to the safety of batteries. In conventional lithium-ion batteries, graphite can pose a safety issue during a fast lithiation process; the overpotential arising from the high current can lead to lithium metal plating on the electrode, which is highly detrimental.[38,39] The fast insertion kinetics of the co-intercalation in graphite can be considered a merit to prevent such situations. Moreover, the relatively high redox potential (>0.3 V vs Li) of the co-intercalation, far greater than the lithium metal formation potential, further precludes lithium metal plating,[21] which was also experimentally confirmed by surface observation of graphite using SEM after fast discharging (Figure S14, Supporting Information). As will be discussed later, the lack of thick SEI layers on the graphite anode cycled with the ether-based electrolyte also aids in enhancing the safety properties of a graphite anode using co-intercalation.[40,41]

The high rate capability of [Li–DEGDME]$^+$ complex ion intercalation in the graphite electrode is unusual considering the large size of the complex ion. To better understand this phenomenon, we considered the possible factors assisting the fast complex ion intercalation kinetics in graphite. In general, guest ion intercalation in electrochemical cells occurs in the following four steps: (i) guest ion diffusion in the electrolyte, (ii) desolvation process at the interface between the electrolyte and electrode, (iii) guest ion diffusion through the SEI layer, and (iv) bulk diffusion in the active electrode material.[42] For (i), we simply compared the ionic conductivities of 1 M LiTFSI in EC/DMC and DEGDME (see the Experimental Section for detailed information). According to our measurements, the ionic conductivities of the two electrolytes were 10.75 ± 0.99 and 9.56 ± 0.16 mS cm^{-1}, respectively, which are consistent with previous reports.[43,44] The marginally similar ionic conductivities indicate that the ionic conductivity of the electrolyte is not a determining factor for the distinctive kinetics. To estimate the effect of (ii), the energy barriers of the desolvation process were comparatively calculated for DEGDME, DMC, and EC solvations (**Figure 5**a). The desolvation energy was estimated based on the energy required for a lithium ion to remove a solvent molecule (see the Experimental Section for a detailed description of the calculations).[45,46] Each step in Figure 5a represents the series of energies required to desolvate the multiple solvation shells. For example, in the bottom panel of Figure 5a, [Li–2EC]$^+$ represents a lithium ion solvated by two EC molecules, and 1.748 eV is the energy necessary to remove one EC molecule and form [Li–EC]$^+$. The first solvation (or last desolvation) energy is significantly higher for DEGDME (3.730 eV) than for DMC

(2.091 eV) or EC (2.384 eV), indicating that the lithium ion and DEGDME solvent are strongly bound to each other, promoting the co-intercalation.[31] This finding is consistent with the experimentally observed [Li–DEGDME]$^+$ co-intercalation phenomena in graphite. Thus, we considered the second-last energy barrier in the DEGDME system to be the effective desolvation energy (1.434 eV), whereas the last energy barriers with the highest values were considered the desolvation energies for DMC (2.091 eV) and EC (2.384 eV) because of their conventional intercalation (highlighted in red in Figure 5a). The energies required to desolvate EC or DMC solvents are much higher than that of DEGDME solvent desolvation by ≈0.7–1 eV, which implies that the desolvation of lithium ions in EC or DMC for the intercalation of graphite will be relatively slower than the desolvation kinetics of the co-intercalation in DEGDME.

We further characterized the SEI layers of the graphite electrodes, which can affect the intercalation kinetics, using transmission electron microscopy (TEM) and XPS. Interestingly, the TEM results indicated that no noticeable SEI layer was formed at the surface of the graphite cycled with 1 M LiTFSI in DEGDME (Figure 5b), whereas a thick amorphous-like SEI layer was commonly observed at the surface of graphite cycled with 1 M LiTFSI in EC/DMC (Figure 5c). The XPS results with depth profiling also clearly confirmed that the SEI layer does not form on the surface of the graphite anode in the DEGDME electrolyte system (Figure 5d). This result contrasts with that for the EC/DMC electrolyte system (Figure 5e), which has typical compounds constituting the SEI such as Li_2CO_3 or $(CH_2OCO_2Li)_2$ and C—O-containing materials.[41] It is believed that the absence of the surface film for the co-intercalation is partly due to the relatively high voltage cut-off of the co-intercalation in the discharge (0.3 V vs Li) and the high LUMO level of the ether solvent, which prevents the reduction of the electrolyte. This result is similar to that for a LTO electrode, which does not generally form a surface film when used as an anode because of its high redox potential.[47,48] Moreover, we speculate that the absence of an apparent desolvation process in the co-intercalation may have contributed to preventing the formation of thick SEI layers; however, further investigation is necessary. The lack of the typical SEI layers at the surface would enable the facile transport of [lithium–ether]$^+$ complex ions into the graphite.

Finally, to understand the bulk diffusion in the electrode during the electrochemical reaction, we probed the electrochemical response of the [lithium–ether]$^+$ complex ion intercalation using cyclic voltammetry (CV) with scan rates from 0.2 to 3 mV s^{-1}, as shown in Figure 5f. Here, it was assumed that the scan rate and peak current follow a power-law equation

$$i = av^b \tag{1}$$

where i is the measured peak current, v is the voltage sweep rate, and a and b are adjustable parameters.[49] A b value of 0.5 generally indicates a diffusion-controlled reaction, whereas a b value of 1 indicates a capacitive reaction.[50] We calculated the b values of every peak in the [lithium–ether]$^+$ complex intercalation by plotting log (scan rate) versus log (peak current), as shown in Figure 5g. To our surprise, a significant pseudocapacitive nature was revealed for the [lithium–ether]$^+$ complex intercalation, in contrast to the charge storage

**ADVANCED
SCIENCE NEWS**

www.advancedsciencenews.com
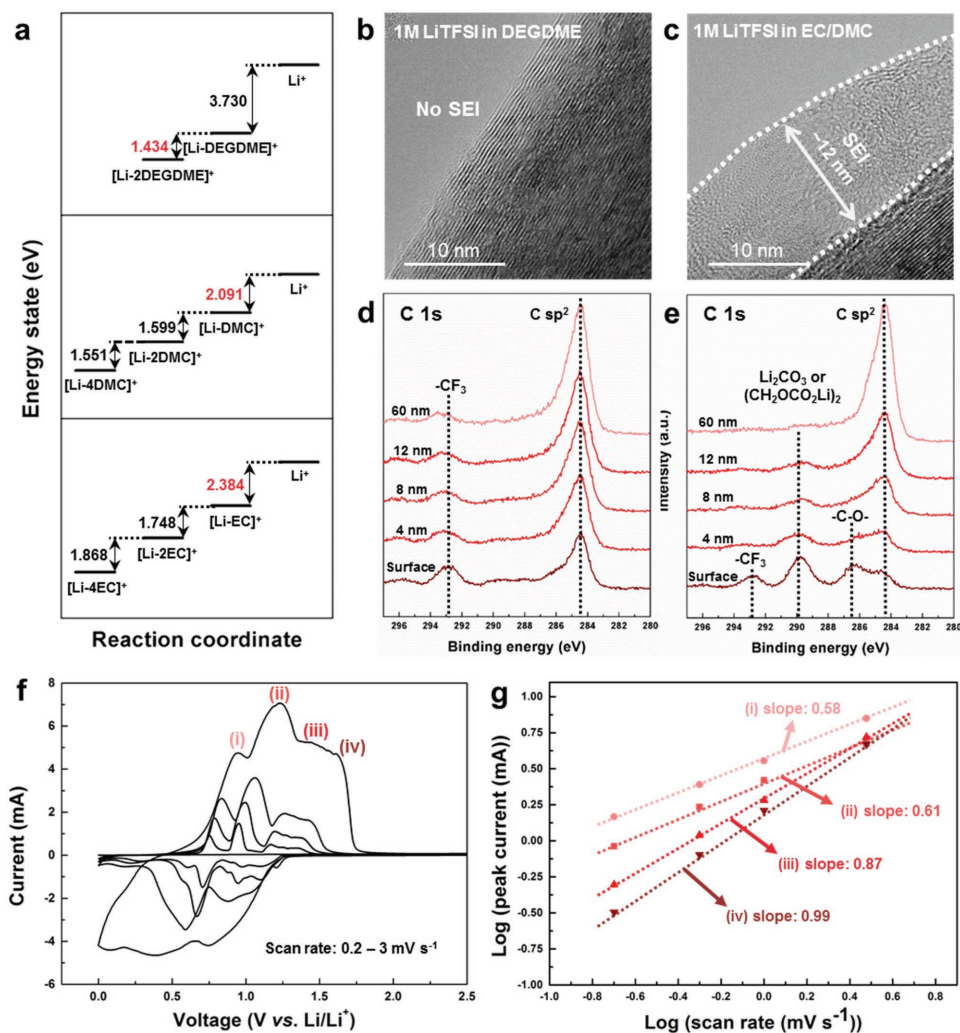
**ADVANCED
ENERGY
MATERIALS**

www.advenergymat.de

Figure 5. Origin of the high rate capability for [lithium–ether]+ co-intercalation. a) Desolvation energy of Li ion solvated with EC, DMC, and DEGDME. b,c) TEM images and d,e) XPS analyses characterizing the edge of graphite cycled with 1 M LiTFSI in DEGDME (left) and 1 M LiTFSI in EC/DMC (1:1, v/v) (right). The XPS CF_3 signal originates from the poly(vinylidene) fluoride binder. f) Cyclic voltammogram of natural graphite using 1 M LiTFSI in DEGDME electrolyte. g) Anodic peak current dependence on the scan rate derived from CV and used to determine the capacitive and intercalation contributions to energy storage.

behavior of conventional lithium ion intercalation, which is mostly diffusion controlled.[51] The *b* values of the peaks were estimated to be 0.99, 0.87, 0.61, and 0.58, respectively, indicating a mixed pseudocapacitive and diffusion reaction, or previously reported partial intercalation pseudocapacitance, during the electrochemical response.[52–56] Considering the apparent first-order phase transition of the [lithium–ether]+ complex in the bulk graphite, as evidenced in the ex situ XRD patterns in Figure 1d, the precise origin of this behavior has not yet been clearly understood. However, this behavior implies that [lithium–ether]+ complex ion diffusion in the graphite galleries promotes faster kinetics compared to conventional lithium ion intercalation. The enlarged space of the co-intercalated graphite with a large amount of the [lithium–ether]+ complex might have a similar lithium insertion local environment to those of the expanded graphite or restacked graphene, which may induce the pseudocapacitive behavior for the intercalation. Also, similar observations have been reported in such as mesoporous

MoS_2,[52] MoO_{3-x},[53] MoS_2 nanocrystal,[54] nanosized-MoO_2,[55] and TiS_2 nanocrystals,[56] which were ascribed to the intercalation pseudocapacitance resulting from the suppressing intercalation-induced phase transitions. In addition, we speculate that the unusually large distance between graphene layers triggered by the initial co-intercalation of the [lithium–ether]+ complex promotes the subsequent co-intercalation of the complex ions with a nonlimited diffusion nature. In this case, the [lithium–ether]+ co-intercalation would exhibit a capacitive behavior with much improved kinetics, which is similar to the unusually fast charge storage mechanism and CV response demonstrated by Dunn and co-workers for an orthorhombic Nb_2O_5 electrode.[50]

3. Conclusion

We demonstrated for the first time that lithium ion/solvent co-intercalation into a graphite electrode can be highly reversible in lithium cells, which can exhibit promising electrochemical

performance with unexpected high power capability. The chemical compatibility of the solvent molecule with the pristine graphite was shown to critically affect the stable co-intercalation. Furthermore, we revealed that the severe capacity degradation previously observed for co-intercalation in a graphite electrode does not stem from the co-intercalation itself but simply results from the chemical instability of the lithium metal in the ether-based electrolyte system. Accordingly, complex ion co-intercalation in a graphite electrode was successfully utilized in both half cells with protected lithium metal and full cells with excellent reversibility. Compared with conventional lithium ion intercalation, the graphite electrode based on the co-intercalation was capable of delivering an impressively higher power capability, retaining more than 87% of its theoretical capacity at a current density of 1 A g^{-1} without the risk of lithium metal plating. Based on combined first-principles calculations and experiments, this higher power capability was attributed to faster desolvation kinetics, the negligible presence of a SEI layer on the graphite electrode, and the diffusion-less charge storage mechanism. Considering the high power capability and expected safety enhancement, co-intercalation-based graphite electrodes may offer an alternative direction for the utilization of graphite in high-power lithium-ion batteries, and this work constitutes the first step toward this advancement.

4. Experimental Section

Materials: Natural graphite (average size: ≈100 μm) was purchased from Bay Carbon Inc. and used without any modification. Electrolytes were carefully prepared to maintain low H$_2$O content (<20 ppm). Lithium salts (LiTF and LiTFSI) and molecular sieves were stored in a vacuum oven at 180 °C. Dried lithium salts were dissolved in a DEGDME solvent at 1 M. The solution was stirred at 80 °C for 3 d. Molecular sieves were added in the solution to remove residual H$_2$O from the electrolyte solution.

Electrode Preparation and Electrochemical Measurements: Graphite electrodes were prepared by mixing the active material (natural graphite, 90 wt%) with polyvinylidene fluoride binder (10 wt%) in an *N*-methyl-2-pyrrolidone solvent. The resulting slurry was uniformly pasted onto Cu foil, dried at 120 °C for 1 h and roll-pressed. The average electrode thickness and loading density were ≈50 μm and ≈5 mg cm^{-2}. Test cells were assembled in a glove box into a two-electrode configuration with a lithium metal counter electrode. Full cells were constructed with excessive amount of LiFePO$_4$ as a cathode material. A separator of grade GF/F (Whatman, USA) was sonicated in acetone and dried at 120 °C before use. Electrochemical profiles were obtained over a voltage range of 2.5 to 0.01 V using a multichannel potentiogalvanostat (WonATech).

Characterization: The structure of the samples was analyzed using an XRD (D2PHASER, Bruker, USA) using Cu Kα radiation. The morphology of the samples was verified using field-emission scanning electron microscopy (SUPRA 55VP, Carl Zeiss, Germany). The electrode after cycling was analyzed using XPS (PHI 5000 VeraProbe) and Raman spectroscopy (high resolution dispersive Raman microscope, Horiba Jobin Yvon, France). Gas evolution during battery operation was characterized using differential electrochemical mass spectrometry (HPR-20, Hiden Analytical). SEI was observed using high-resolution TEM (JEM2100F, JEOL, Japan). Ionic conductivity of electrolytes was measured with portable conductivity meter (Oakton waterproof portable CON 610 conductivity meter, Singapore).

Calculation Details: First-principles calculations were conducted to obtain the HOMO/LUMO levels and the energy of [Li–solvent$_x$]$^+$ complexes (solvents: PC, EC, DMC, and DEGDME) and isolated solvent molecules using the Gaussian 09 code.[57] All geometries were optimized with the B3LYP/6-311G (3df) level of exchange-correlation functionals and basis sets.[58,59] Based on the calculated energies of molecules, desolvation energy E_{des} was obtained using the following definition: $E_{des,x} = E_{[Li-solvent_{x-1}]^+} + E_{solvent} - E_{[Li-solvent_x]^+}$. Here, $E_{[Li-solvent_{x-1}]^+}$, $E_{[Li-solvent_x]^+}$, and $E_{solvent}$ represent the energy of [Li–solvent$_{x-1}$]$^+$, [Li–solvent$_x$]$^+$, and isolated solvent molecule, respectively.

Supporting Information

Supporting Information is available from the Wiley Online Library or from the author.

Conflict of Interest

The authors declare no conflict of interest.

Keywords

[1] L. B. Ebert, *Ann. Rev. Mater. Sci.* **1976**, *6*, 181.

[2] Y. Nishi, *J. Power Sources* **2001**, *100*, 101.

[3] F. Cao, I. V. Barsukov, H. J. Bang, P. Zaleski, J. Prakash, *J. Electrochem. Soc.* **2000**, *147*, 3579.

[4] M. Yoshio, H. Wang, K. Fukuda, *Angew. Chem.* **2003**, *115*, 4335.

[5] T. Tsumura, A. Katanosaka, I. Souma, T. Ono, Y. Aihara, J. Kuratomi, M. Inagaki, *Solid State Ionics* **2000**, *135*, 209.

[6] Y. Kobayashi, H. Miyashiro, K. Kumai, K. Takei, T. Iwahori, I. Uchida, *J. Electrochem. Soc.* **2002**, *149*, A978.

[7] D. Aurbach, E. Zinigrad, Y. Cohen, H. Teller, *Solid State Ionics* **2002**, *148*, 405.

[8] J.-i. Yamaki, H. Takatsuji, T. Kawamura, M. Egashira, *Solid State Ionics* **2002**, *148*, 241.

[9] M. Winter, G. H. Wrodnigg, J. O. Besenhard, W. Biberacher, P. Novák, *J. Electrochem. Soc.* **2000**, *147*, 2427.

[10] M. Ishikawa, T. Sugimoto, M. Kikuta, E. Ishiko, M. Kono, *J. Power Sources* **2006**, *162*, 658.

[11] D. Aurbach, Y. Ein-Eli, B. Markovsky, A. Zaban, S. Luski, Y. Carmeli, H. Yamin, *J. Electrochem. Soc.* **1995**, *142*, 2882.

[12] R. McMillan, H. Slegr, Z. X. Shu, W. Wang, *J. Power Sources* **1999**, *81-82*, 20.

[13] P. Arora, R. E. White, M. Doyle, *J. Electrochem. Soc.* **1998**, *145*, 3647.

[14] B. P. Sullivan, *J. Electrochem. Soc.* **1970**, *117*, 222.

[15] M. Arakawa, J.-I. Yamaki, *J. Electroanal. Chem. Interfacial Electrochem.* **1987**, *219*, 273.

ADVANCED
SCIENCE NEWS
www.advancedsciencenews.com

ADVANCED
ENERGY
MATERIALS
www.advenergymat.de

[16] H. Moon, R. Tatara, T. Mandai, K. Ueno, K. Yoshida, N. Tachikawa, T. Yasuda, K. Dokko, M. Watanabe, *J. Phys. Chem. C* **2014**, *118*, 20246.

[17] Y. Yamada, K. Usui, C. H. Chiang, K. Kikuchi, K. Furukawa, A. Yamada, *ACS Appl. Mater. Interfaces* **2014**, *6*, 10892.

[18] T. Abe, N. Kawabata, Y. Mizutani, M. Inaba, Z. Ogumi, *J. Electrochem. Soc.* **2003**, *150*, A257.

[19] X.-R. Liu, L. Wang, L.-J. Wan, D. Wang, *ACS Appl. Mater. Interfaces* **2015**, *7*, 9573.

[20] H. Kim, J. Hong, Y.-U. Park, J. Kim, I. Hwang, K. Kang, *Adv. Funct. Mater.* **2015**, *25*, 534.

[21] B. Jache, P. Adelhelm, *Angew. Chem., Int. Ed.* **2014**, *53*, 10169.

[22] Z. Zhu, F. Cheng, Z. Hu, Z. Niu, J. Chen, *J. Power Sources* **2015**, *293*, 626.

[23] B. Jache, J. O. Binder, T. Abe, P. Adelhelm, *Phys. Chem. Chem. Phys.* **2016**, *18*, 14299.

[24] P. Han, X. Han, J. Yao, L. Zhang, X. Cao, C. Huang, C. Gui, *J. Power Sources* **2015**, *297*, 457.

[25] P. Han, X. Han, J. Yao, Z. Liu, X. Cao, G. Cui, *Electrochem. Commun.* **2015**, *61*, 84.

[26] H. Kim, G. Yoon, K. Lim, K. Kang, *Chem. Commun.* **2016**, *52*, 12618.

[27] C. Gejke, L. Börjesson, K. Edström, *Electrochem. Commun.* **2003**, *5*, 27.

[28] A. M. Andersson, M. Herstedt, A. G. Bishop, K. Edström, *Electrochim. Acta* **2002**, *47*, 1885.

[29] H. Kim, J. Hong, G. Yoon, H. Kim, K.-Y. Park, M.-S. Park, W.-S. Yoon, K. Kang, *Energ. Environ. Sci.* **2015**, *8*, 2963.

[30] G. C. Chung, H. J. Kim, S. I. Yu, S. H. Jun, J. w. Choi, M. H. Kim, *J. Electrochem. Soc.* **2000**, *147*, 4391.

[31] G. Yoon, H. Kim, I. Park, K. Kang, *Adv. Energy Mater.* **2017**, *7*, 1601519.

[32] M. Shiraishi, M. Ata, *Carbon* **2001**, *39*, 1913.

[33] Y. Yamada, A. Yamada, *J. Electrochem. Soc.* **2015**, *162*, A2406.

[34] J. Qian, W. A. Henderson, W. Xu, P. Bhattacharya, M. Engelhard, O. Borodin, J.-G. Zhang, *Nat. Commun.* **2015**, *6*, 6362.

[35] D. Aurbach, E. Pollak, R. Elazari, G. Salitra, C. S. Kelley, J. Affinito, *J. Electrochem. Soc.* **2009**, *156*, A694.

[36] X. Liang, Z. Wen, Y. Liu, M. Wu, J. Jin, H. Zhang, X. Wu, *J. Power Sources* **2011**, *196*, 9839.

[37] Y. Kim, K.-H. Ha, S. M. Oh, K. T. Lee, *Chem. - Eur. J.* **2014**, *20*, 11980.

[38] A. Same, V. Battaglia, H.-Y. Tang, J. Park, *J. Appl. Electrochem.* **2012**, *42*, 1.

[39] I. Belharouak, G. M. Koenig Jr., K. Amine, *J. Power Sources* **2011**, *196*, 10344.

[40] Z. Zhang, D. Fouchard, J. R. Rea, *J. Power Sources* **1998**, *70*, 16.

[41] P. Verma, P. Maire, P. Novák, *Electrochim. Acta* **2010**, *55*, 6332.

[42] K. Xu, A. von Cresce, U. Lee, *Langmuir* **2010**, *26*, 11538.

[43] A. Ponrouch, E. Marchante, M. Courty, J.-M. Tarascon, M. R. Palacin, *Energy Environ. Sci.* **2012**, *5*, 8572.

[44] B. Garcia, S. Lavallée, G. Perron, C. Michot, M. Armand, *Electrochim. Acta* **2004**, *49*, 4583.

[45] T. Abe, H. Fukuda, Y. Iriyama, Z. Ogumi, *J. Electrochem. Soc.* **2004**, *151*, A1120.

[46] J. Zheng, Y. Hou, Y. Duan, X. Song, Y. Wei, T. Liu, J. Hu, H. Guo, Z. Zhuo, L. Liu, Z. Chang, X. Wang, D. Zherebetskyy, Y. Fang, Y. Lin, K. Xu, L.-W. Wang, Y. Wu, F. Pan, *Nano Lett.* **2015**, *15*, 6102.

[47] I. Belharouak, Y.-K. Sun, W. Lu, K. Amine, *J. Electrochem. Soc.* **2007**, *154*, A1083.

[48] Y.-Q. Wang, L. Gu, Y.-G. Guo, H. Li, X.-Q. He, S. Tsukimoto, Y. Ikuhara, L.-J. Wan, *J. Am. Chem. Soc.* **2012**, *134*, 7874.

[49] J. Wang, J. Polleux, J. Lim, B. Dunn, *J. Phys. Chem. C* **2007**, *111*, 14925.

[50] V. Augustyn, J. Come, M. A. Lowe, J. W. Kim, P.-L. Taberna, S. H. Tolbert, H. D. Abruña, P. Simon, B. Dunn, *Nat. Mater.* **2013**, *12*, 518.

[51] M. D. Levi, D. Aurbach, *J. Electroanal. Chem.* **1997**, *421*, 79.

[52] J. B. Cook, H.-S. Kim, Y. Yan, J. S. Ko, S. Robbennolt, B. Dunn, S. H. Tolbert, *Adv. Energy Mater.* **2016**, *6*, 1501937.

[53] H.-S. Kim, J. B. Cook, H. Lin, J. S. Ko, S. H. Tolbert, V. Ozolins, B. Dunn, *Nat. Mater.* **2017**, *16*, 454.

[54] J. B. Cook, H.-S. Kim, T. C. Lin, C.-H. Lai, B. Dunn, S. H. Tolbert, *Adv. Energy Mater.* **2017**, *7*, 1601283.

[55] H.-S. Kim, J. B. Cook, S. H. Tolbert, B. Dunn, *J. Electrochem. Soc.* **2015**, *162*, A5083.

[56] G. A. Muller, J. B. Cook, H.-S. Kim, S. H. Tolbert, B. Dunn, *Nano Lett.* **2015**, *15*, 1911.

[57] M. J. Frisch, G. W. Trucks, H. B. Schlegel, G. E. Scuseria, M. A. Robb, J. R. Cheeseman, G. Scalmani, V. Barone, B. Mennucci, G. A. Petersson, H. Nakatsuji, M. Caricato, X. Li, H. P. Hratchian, A. F. Izmaylov, J. Bloino, G. Zheng, J. L. Sonnenberg, M. Hada, M. Ehara, K. Toyota, R. Fukuda, J. Hasegawa, M. Ishida, T. Nakajima, Y. Honda, O. Kitao, H. Nakai, T. Vreven, J. A. Montgomery Jr., J. E. Peralta, F. Ogliaro, M. J. Bearpark, J. Heyd, E. N. Brothers, K. N. Kudin, V. N. Staroverov, R. Kobayashi, J. Normand, K. Raghavachari, A. P. Rendell, J. C. Burant, S. S. Iyengar, J. Tomasi, M. Cossi, N. Rega, N. J. Millam, M. Klene, J. E. Knox, J. B. Cross, V. Bakken, C. Adamo, J. Jaramillo, R. Gomperts, R. E. Stratmann, O. Yazyev, A. J. Austin, R. Cammi, C. Pomelli, J. W. Ochterski, R. L. Martin, K. Morokuma, V. G. Zakrzewski, G. A. Voth, P. Salvador, J. J. Dannenberg, S. Dapprich, A. D. Daniels, Ö. Farkas, J. B. Foresman, J. V. Ortiz, J. Cioslowski, D. J. Fox, *Gaussian, Inc.*, Wallingford, CT **2009**.

[58] A. D. Becke, *J. Chem. Phys.* **1993**, *98*, 5648.

[59] A. McLean, G. Chandler, *J. Chem. Phys.* **1980**, *72*, 5639.